https://doi.org/10.5194/egusphere-2022-658
Preprint. Discussion started: 25 July 2022

A new analytical method for stability analysis of rock blocks with cavity in sub-horizontal strata by considering eccentric effect

Xushan Shi[1], Bo Chai[1,3,4], Juan Du[1,2,4], Wei Wang[1,3,4], Bo Liu[1]

[1]School of Environmental Studies, China University of Geosciences, Wuhan, 430078, China
[2]Centre for severe weather and climate and hydro-geological hazards, Wuhan, 430078, China
[3]Hubei Key Laboratory of Yangtze Catchment Environmental Aquatic Science, Wuhan, 430078, China
[4] Research Center for Geohazards Monitoring and Warning in Three Gorges Reservoir, Wanzhou, 404000, China

Correspondence to: Bo Chai (chaibo@cug.edu.cn) and Juan Du (dujuan@cug.edu.cn)

Abstract. The basal cavity of rock block formed due to differential weathering is an important predisposing factor for rockfall, in hard-soft interbedded rocks. The rock block falling due to eccentric effect with the failure modes of toppling or sliding is defined as biased rockfall in this study. Considering the non-uniform stress distribution due to eccentric effect, a new analytical method for three-dimensional stability analysis of biased rockfall is proposed. In addition, a set of factors of safety (Fos) against partial damage (compressive and tensile damage of soft underlying layer) and overall failure (toppling and sliding of hard rock block) are used to determine the rockfall susceptibility level. The analytical method was applied and validated with the biased rockfalls in the northeast edge of Sichuan basin in Southwest China, where a large amounts of rockfalls develops, composed of overlying thick sandstone and underlying mudstone. The evolution process of biased rockfalls is divided into four stages, initial state, cavity formation, partial unstable and failure. The proposed method is validated by calculating Fos of the typical unstable rock blocks in the study area. It is indicated that the continuous retreat of cavity causes the stress redistribution between hard and soft rock layers. Consequently, the development of eccentric effect leads to the damage of underlying soft rock layer and the further failure of hard rock block. The critical cavity retreat ratio is determined as 0.33 to classify the low and moderate rockfall susceptibility. The proposed analytical method is effective for the early identification of biased rockfall, which is significant for rockfall prevention and risk mitigation.

List of symbols

a	length of the block along the x direction
A	area of contact surfaces
b	width of the block along the y direction
c	cohesive force of the mudstone
d_i	width of the basal cavity in a certain direction
e_x	eccentric distance along the x direction
e_y	eccentric distance along the y direction
E_x	horizontal seismic force along x direction

https://doi.org/10.5194/egusphere-2022-658
Preprint. Discussion started: 25 July 2022

Fos	factor of safety
h	height of the block
h_w	height of the water in the fracture
H_x	water pressure along x direction
I_x	moment of inertia with respect to x-axis
I_y	moment of inertia with respect to y-axis
k_e	earthquake contribution coefficient
M_{bx}	total bending moments with respect to the x-axis on the mudstone foundation
M_{by}	total bending moments with respect to the y-axis on the mudstone foundation
M_{bEx}	bending moment of E_x with respect to the x-axis on the mudstone foundation
M_{bHx}	bending moment of H_x with respect to the x-axis on the mudstone foundation
M_{bWx}	bending moment of W with respect to the x-axis on the mudstone foundation
M_{Ex}	overturning moment provided by E_x along x direction
M_{Hx}	overturning moment provided by H_x along x direction
M_{px}	stabilizing moment of p_n along x direction
$M_{W_{inx}}$	stabilizing moment provided by W along x direction
$M_{W_{outx}}$	overturning moment provided by W along x direction
N_z	total applied vertical load on the mudstone base
O	origin of the (x, y) coordinates
$p(x,y)$	pressure magnitude at point (x,y)
r_i	the basal cavity retreat ratio equal to the ratio of cavity width to block width in a certain direction
W	weight of the block
x	distance to O along the x-axis
y	distance to O along the y-axis
α	true dip of the contact surface
γ_s	unit weight of sandstone
γ_w	unit weight of water
θ_1	apparent dip of α on the plane J1
θ_2	apparent dip of α on the plane J2
σ_{cmax}	ultimate tensile strength of the mudstone
σ_{tmax}	ultimate tensile strength of the mudstone
τ_{max}	ultimate Shear Strength of the mudstone
φ	friction angle of the mudstone

https://doi.org/10.5194/egusphere-2022-658
Preprint. Discussion started: 25 July 2022

ω_1 angle between the trend of the contact surface and the x direction

ω_2 angle between the trend of the contact surface and the y direction

1 Introduction

Rockfall is defined as the detachment of a rock block from a steep slope along a surface, on which little or no shear displacement takes place (Cruden and Varnes, 1996). Rockfalls frequently occur in mountainous ranges, cut slopes, and coastal cliffs, and they may cause significant facilities damage and casualties in residential areas and transport corridors (Chau et al., 2003; Volkwein et al., 2011; Corominas et al., 2018). Stability and failure probability of rock blocks are crucial for risk management and early warning of rockfall (Kromer et al., 2017).

Rockfall is widespread and poses high risk in the eastern Sichuan Basin, southwest China (Chen et al., 2008; Chen and Tang, 2010; Zhang et al., 2016; Zhou et al., 2017; Zhou et al., 2018). The rockfall in this area is attributed to the tectonic setting of Jura-type folds and the stratum sequence, which is characterized by the interbedding of hard and soft layers. An alternation of thick sandstone and thin mudstone layers are formed in the wide and gentle-angle synclines (Zhang et al., 2015; Wu et al., 2018). Weathering is known to be one of the main factors (Jaboyedoff et al., 2021; Zhan et al., 2022). The cliff comprised of hard sandstone is the source of rockfall, and the underlying mudstone is more susceptible to weathering. Along with the extending of basal cavities in mudstone layer, the overlying sandstone blocks gradually become unstable because of the eccentric effect, which could fail with the mode of toppling or sliding. This type of rockfall is defined as biased rockfall in this study (Fig. 1). Similar rockfall patterns have been widely reported in other regions, such as Joss Bay in England (Hutchinson, 1972), Okinawa Island in Japan (Kogure et al., 2006), and the Colorado Plateau of the southwestern United States (Ward et al., 2011). Extending of basal cavity is a main cause for the failure of overlying block. Therefore, it is necessary to establish an analytical method, considering the development of basal cavity, to analyze the stress distribution and stability of rock blocks, which is fundamental to the susceptibility assessment and risk control of biased rockfall.

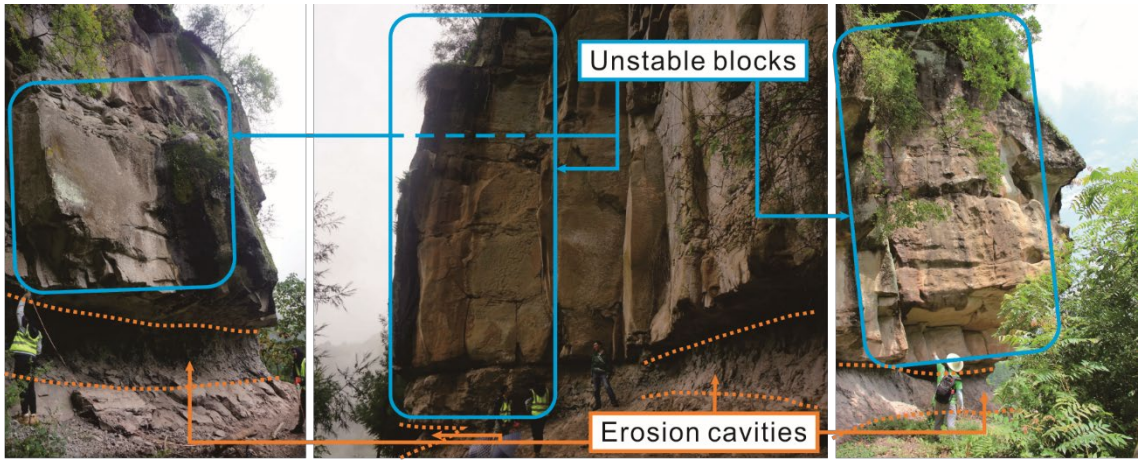

Figure 1 Unstable blocks and basal cavities caused by differential weathering.

https://doi.org/10.5194/egusphere-2022-658
Preprint. Discussion started: 25 July 2022

Rockfall stability analysis methods include statistical analysis (Frattini et al., 2008; Santi et al., 2009), empirical rating systems (Pierson et al., 1990; Ferrari et al., 2016), and mechanical analysis (Jaboyedoff et al., 2004; Derron et al., 2005; Matasci et al., 2018). The statistical analysis and empirical rating systems are suitable for rockfall hazard assessment at a regional scale. The accuracy of statistical analysis depends on the completeness of rockfall inventories (Chau et al., 2003; Guzzetti et al., 2003; D'amato et al., 2016). However, its application to rockfall hazards is limited due to the absence of inventory data (Budetta and Nappi, 2013; Malamud et al., 2004). Empirical and semi-empirical rating systems are used where site-specific rockfall inventories are either unavailable or unreliable. Therefore, rockfall susceptibility can be assessed by heuristic ranking of selected predisposing factors (Frattini et al., 2008; Budetta, 2004). Mechanical analysis based on static equilibrium theory is the main method to analyze the stability of site-specific rockfall using the factor of safety (Fos). Ashby (1971) has conducted stability analysis with parallelepiped block resting on inclined plane (Fig. 2a), the solution was subsequently modified by Bray and Goodman (1981), and Sagaseta (1986). Kogure et al. (2006) utilized the cantilever beam model to determine the critical state of limestone cliffs. Frayssines and Hantz (2009) proposed the limit equilibrium method (LEM) to predict block stability considering sliding and toppling in steep limestone cliffs (Fig. 2b). Chen and Tang (2010) established a stability analysis method of three types of unstable rocks, in the Three Gorges Reservoir area with the LEM. Alejano et al. (2015) studied the influence of rounding of block corners on the block stability. Zhang et al. (2016) defined Fos based on fracture mechanics and studied the progressive failure process by analyzing crack propagation. Alejano et al. (2010) and Pérez-Rey et al. (2021) deduced the formula for Fos of blocks with more complex geometry.

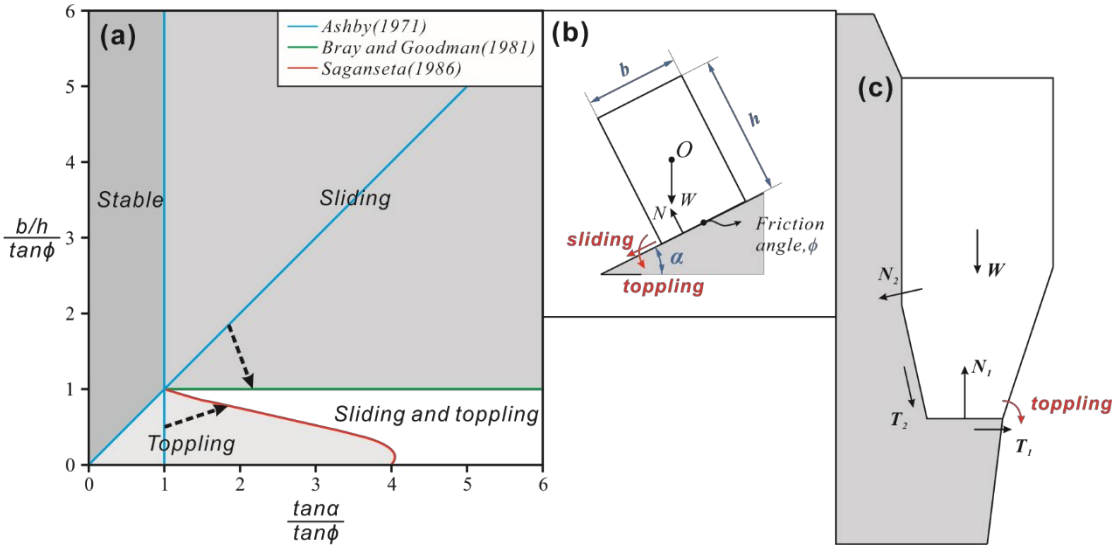

Figure 2 Traditional force analysis diagrams of rock block. (a) and (b) are stability analysis diagrams of rock block in dynamic conditions, resting on an inclined plane with the dip angle of α. The rock block is generalized as cuboid with the dimensions of b × h (as modified from Ashby (1971), Bray and Goodman (1981) and Sagaseta (1986)). (c) Force description of the toppling model proposed by Frayssines and Hantz (2009). In the above assumptions, *N* is regarded as a force applied at a point.

https://doi.org/10.5194/egusphere-2022-658
Preprint. Discussion started: 25 July 2022

The supporting force at the contact surface is assumed to applied at a point in the current LEM methods (i.e., N in Fig. 2 b and c). However, the supporting force is actually a distributed force. The cavity generates eccentric effect on the overlying rock mass and results in non-uniform distribution of supporting force on the contact surface, which is not considered in traditional LEM. Furthermore, most studies simplified the three-dimensional geometry of the slope by cross-section, which is used to represent the critical features of the slope structure. Nevertheless, for natural blocks with basal cavities (Pérez-Rey et al., 2021), the cavities along different directions usually present different depths. Therefore, three-dimensional model is necessary to calculate the accurate stability. Besides, when a block has multiple free faces, it's potential failure will be dominated by different modes, including rock mass damage and overall block failure. Therefore, the probable failure modes should be determined prior to the calculation of Fos.

Based on rockfall investigation in the Eastern Sichuan Basin, China, the main objective of this study was to propose a new three-dimensional method for the determination of failure modes and Fos of biased rockfall, considering the non-uniform force distribution on the contact surfaces. Fos of the typical unstable rock blocks in the study area were calculated to validate the new method. In addition, the critical cavity retreat ratio (r) in this area was given. This study is an extension of basic LEM for rockfall, which could promote the accuracy of rockfall stability analysis and facilitate rockfall prevention and risk mitigation.

2 Study area

2.1 Geological setting

The study area is located in northeast edge of the Sichuan basin, China (Fig. 3a). Continuous erosion processes generate moderate-low mountain and valley landform (Yu et al., 2021). The tectonic structure of this area is characterized by a series of NEE anticlines and synclines (Fig. 3b, c). In the anticlines area, the rock layers dip relatively steeply, where translational rockslide is the main mode of slope failure. The syncline area is dominated by gentle dipping strata and is prone to rockfall (Zhou et al., 2018). The study area is located in the core of Matouchang syncline, where the rock layers are sub-horizontal (Fig. 3d, e). In this valley, due to the longstanding fluvial incision, the relative relief is about 500 m and the valley flanks are extremely steep (Fig. 3e). Besides, the toes of the hill slopes are reshaped because of the construction of G318 national road, which is the main traffic line and always threatened by rockfalls dropping from the steep rock slopes (shown in Fig. 3d and Table 1).

https://doi.org/10.5194/egusphere-2022-658
Preprint. Discussion started: 25 July 2022

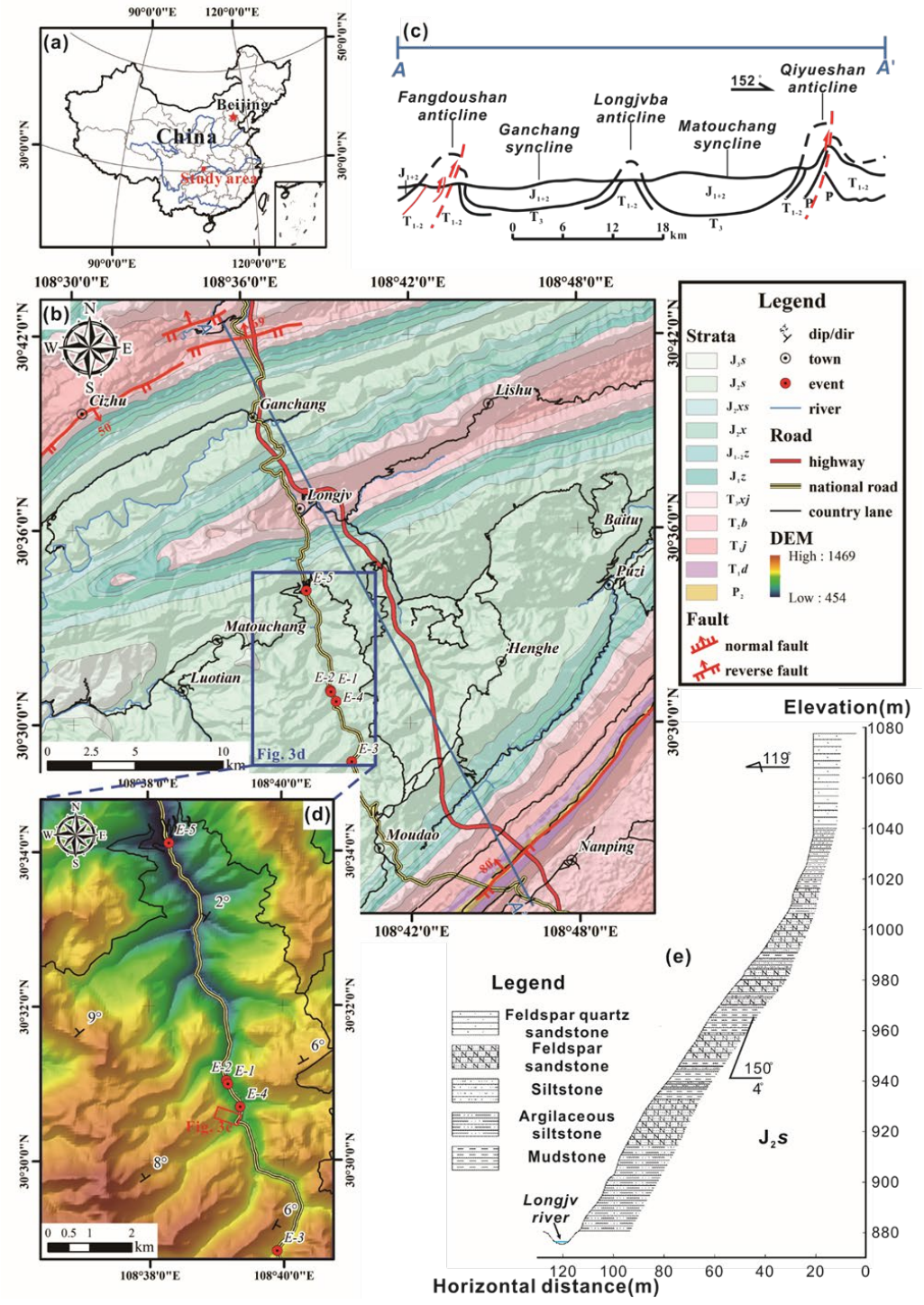

Figure 3 (a) Location of the study area in China; (b) geological map of the study area; (c) tectonic sketch profile of A-A'; (d) rockfall-prone segment and key investigation areas. The red dots are the positions of historical rockfall events, corresponding to the serial numbers

https://doi.org/10.5194/egusphere-2022-658
Preprint. Discussion started: 25 July 2022

in Table 1; (e) Geological cross-section of the hillslope in the Jitougou section of G318 national road, which is marked by a red rectangle in Fig. 3d.

Table 1 Historical rockfall events along G318 national road in the study area

Serial number	Location	Time of occurrence (GMT+8)	Volume [m^3]	Consequence
E-1	K1698+900	2014-05 to 06*	Unknown	The power transmission facilities outside the road were smashed.
E-2	K1699+000	2015-02-14 23:00	About 240	A passing truck was stuck and two people dead.
E-3	K1690+700	2015-06-16	Unknown	The road was interrupted for a day.
E-4	K1698+400	2015-06-18 09:00	About 200	A vehicle was crashed into a gully and four people dead.
E-5	K1741+800	2020-04-21 05:30	About 232000	Eight houses were damaged and a gas station was affected.

*Note: The exact time is unknown.

2.2 Rockfall characteristics

The slopes in the study area have multi-layer unstable rock blocks (Fig. 4a), which are consist of a sub-horizontally interbedding of sandstone and mudstone layers. The thick sandstone has two sets of sub-vertical joint (Fig. 5), which cut the rock mass into blocks as the potential rockfall source (Fig. 4b). Cavities are formed in the underlying mudstone layer (Fig. 4c, d). Joints and bedding plane (BP) constitute the detachment surface between the blocks and steep slope (Fig. 4e). Eccentric effect produced by the mudstone cavity plays an important role in the rockfall process. When the basal mudstone cannot provide adequate supporting force, the blocks detach from steep slope and biased rockfall occurs. There are two possible failure modes of biased rockfall, namely sliding and toppling.

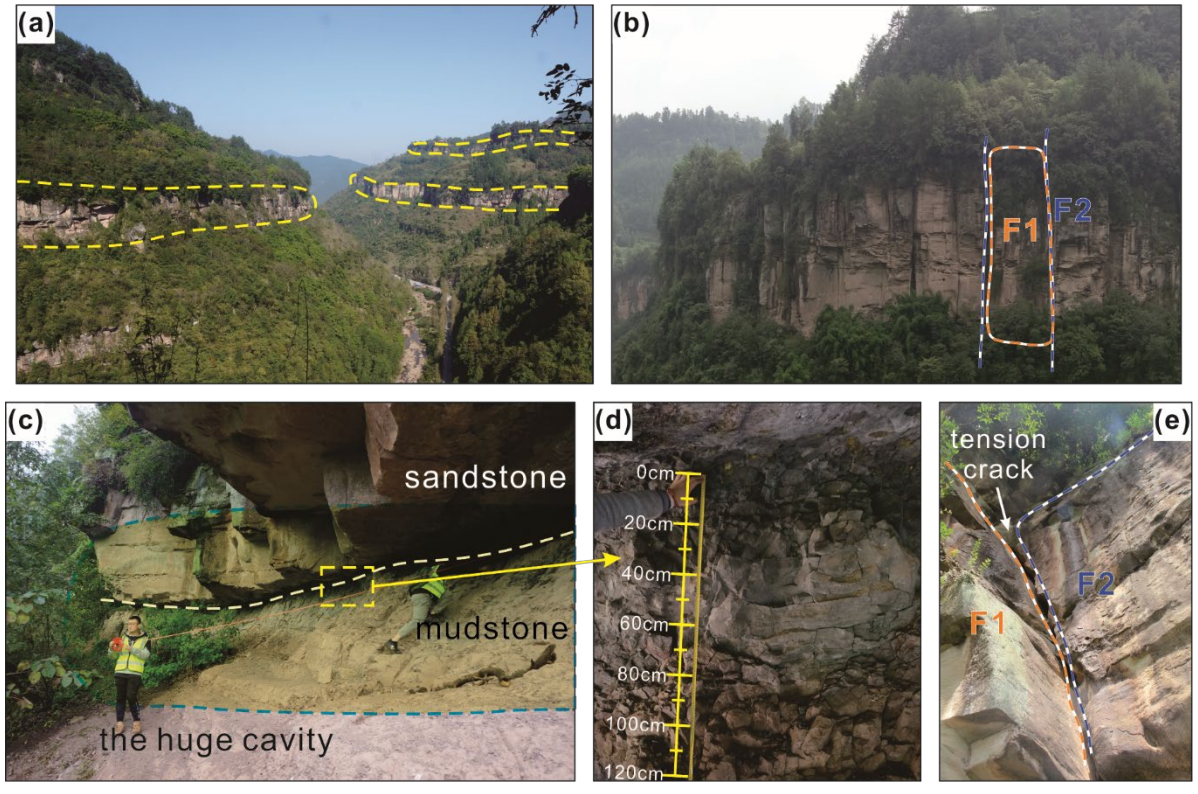

https://doi.org/10.5194/egusphere-2022-658
Preprint. Discussion started: 25 July 2022

Figure 4 Characteristics of biased rockfalls in study area. (a) Multi-layer of rockfall sources, which is consist of thick sandstone. (b) Two sets of sub-vertical joints (F1 and F2) recognized by the UAV photos. (c) A large basal cavity developed in the underlying mudstone. (d) The dense factures on the mudstone surface generated by weathering and compression. (e) A vertical tension crack in the rear of the block through which precipitation can infiltrate.

In the study area, rainfall is the main predisposing factors of rockfall. The precipitation mainly infiltrates along the sub-vertical joints or cracks of the sandstone (Fig. 4e). However, the draining of fissure water is hysteretic due to the obstruction of basal mudstone. Therefore, transient steady flow exists in vertical cracks during heavy rainfall, and the hydrostatic pressure triggers the detachment of rock blocks. Thus, typical scenarios (such as rainfall intensity and earthquake) need to be considered in the stability analysis model.

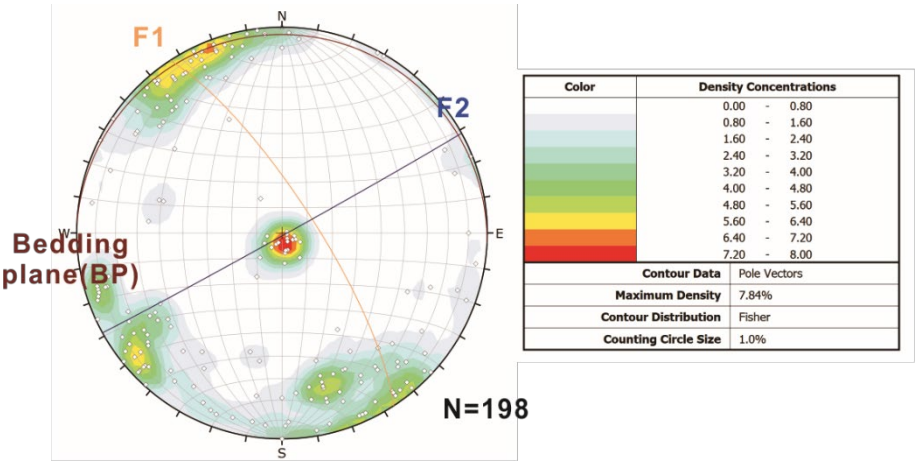

Figure 5 Stereo net produced using compass-clinometer survey data, which shows the densities and orientations of five clusters.

3 Calculation method

3.1 Geological models

A detailed geological investigation for unstable rock blocks were carried out in the study area (Fig. 6). The model of rock block is mainly composed of the overlying sandstone and the underlying mudstone. The sandstone block is assumed to be a rigid body, which is divided by two sets of orthogonal vertical smooth joints without friction resistance. Blocks with multiple free faces are prone to failure. Due to cavity in the mudstone, the contact surface between sandstone and mudstone has an eccentric effect. The underlying mudstone plays the role of a rectangular base, which provides non-uniform distributed forces at different locations. Mudstone is loaded by compressive stress, tensile stress and shear stress, however, it doesn't present deformation. The rock block keeps in the state of static equilibrium prior to the final overall failure. Fig. 7 expresses the four evolution stages of biased rockfall. In the initial stage, the base cavity has not yet formed and the normal force acting on the contact surface is uniform in different positions. Eccentric effect leads to non-uniform supporting force as the

https://doi.org/10.5194/egusphere-2022-658
Preprint. Discussion started: 25 July 2022

cavity grows, partially damage gradually develops until the non-uniform force exceeds the compressive or tensile strength of the mudstone. Under the triggering effects of rainfall or earthquakes, the rock blocks will be separated by sliding or toppling.

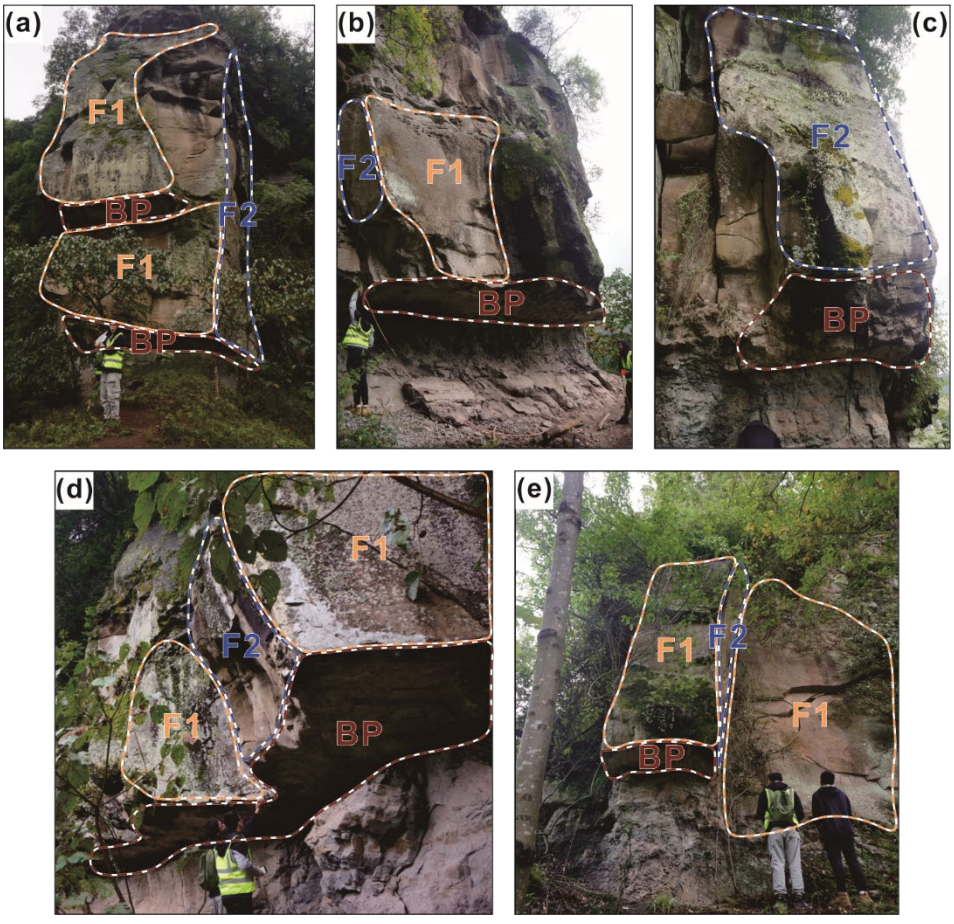

Figure 6 The unstable blocks labelled W02, W08, W18, W04, W21, which are detached by the dominated discontinuities in Fig. 5. Obvious basal cavities can be identified under the bedding planes of sandstone.

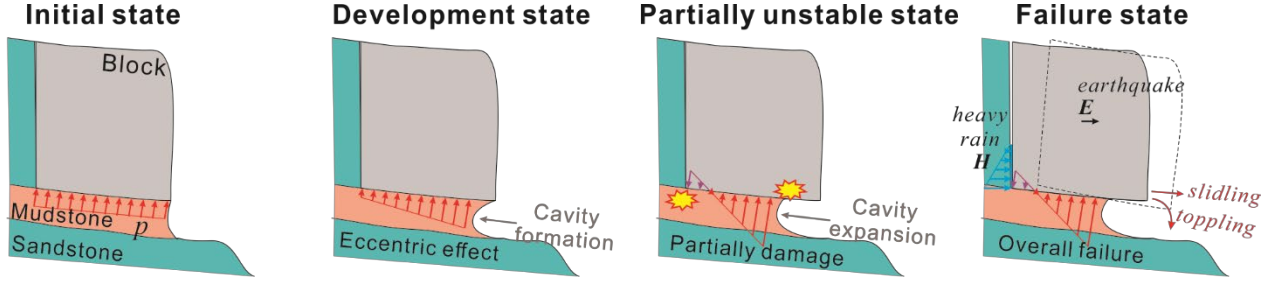

Figure 7 The evolution process of rock blocks from stable state to failure.

Fig. 8 represents the mechanical model of force equilibrium analysis of rock block with two or three free faces. The rock block is generalized as a parallelepiped block. The shear strength of the underlying mudstone is assumed to obeys Mohr-

https://doi.org/10.5194/egusphere-2022-658
Preprint. Discussion started: 25 July 2022

Coulomb criterion. The predisposing factors s of rainfall and earthquake decrease Fos by generating hydrostatic pressure H in the vertical crack and horizontal seismic force E on the block.

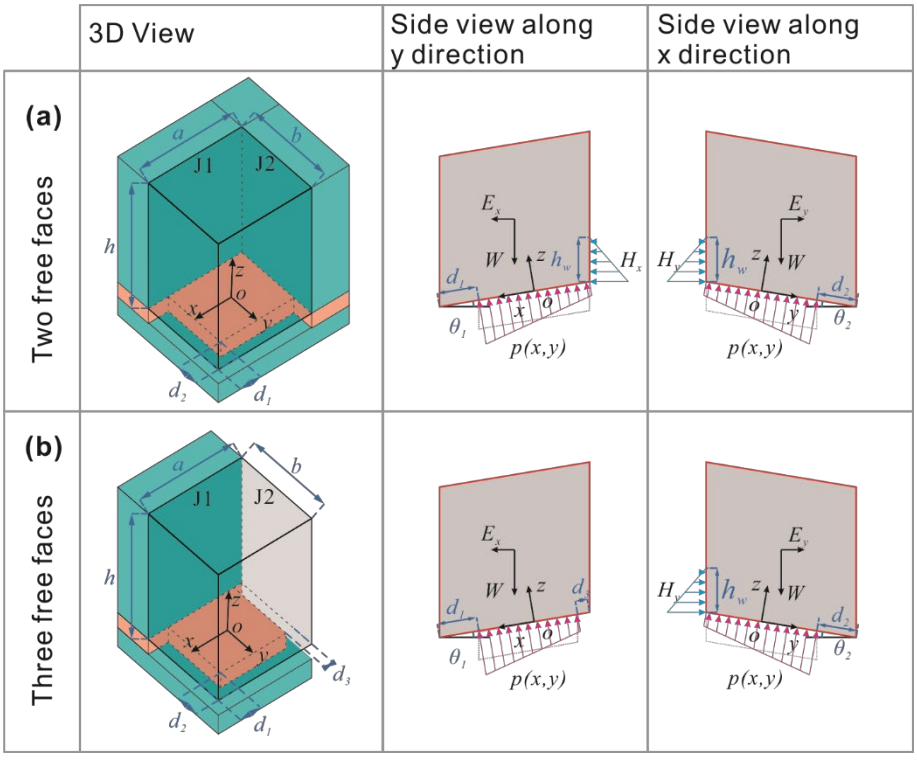

Figure 8 Diagram of force equilibrium analysis of the rock block model. (a) and (b) represent the case of unstable rock blocks with two or three free surfaces, respectively.

3.2 Calculation processes

3.2.1 Distributed force

The following formulas are used to calculate apparent dip of α (θ_1 and θ_2):

$$\theta_1 = \arctan(\tan\alpha \cdot \cos\omega_1) \quad (1)$$

$$\theta_2 = \arctan(\tan\alpha \cdot \cos\omega_2) \quad (2)$$

Where, $\omega_1$and ω_2 are the angles between the trend of the contact surface and the x direction or y direction.

As shown in Fig. 8b, with respect to x-axis, gravity, seismic forces, and hydrostatic pressure create bending moments on the foundation. The bending moment of gravity with respect to x-axis (M_{bWx}) is

$$M_{bWx} = W \cdot \frac{d_1 - d_3}{2} \cos\theta_1 \quad (3)$$

Assume that the height of the water in the fracture is h_w, the hydrostatic pressure along x direction (H_x) and its bending moment (M_{bHx}) are respectively expressed as,

https://doi.org/10.5194/egusphere-2022-658
Preprint. Discussion started: 25 July 2022

$$H_x = \frac{\gamma_w h_w^2}{2}(b - d_2) \tag{4}$$

$$M_{bHx} = \int_{-\frac{b-d_2}{2}}^{\frac{b-d_2}{2}} \int_0^{h_w \cos\theta_1} \gamma_w \left(h_w - \frac{z}{\cos\theta_1}\right)\left(\frac{z}{\cos\theta_1} + \frac{a - d_1 - d_3}{2} \cdot \sin\theta_1\right) dz dy \tag{5}$$

The horizontal seismic force along x direction (E_x) and its bending moment (M_{bEx}) are respectively expressed as,

$$E_x = k_e W \tag{6}$$

$$M_{bEx} = E_x \left(\frac{h}{2} - \frac{d_1 - d_3}{2} \sin\theta_1\right) \tag{7}$$

The total applied vertical load (N_z) and the total bending moments along x direction (M_{bx}) can be derived as,

$$N_z = W \cos\alpha - (H_x \cdot k_1 \cdot k_3 + E_x \cdot k_2) \sin\theta_1 - \left(H_y \cdot k_1 + E_y \cdot k_2\right) \sin\theta_1 \tag{8}$$

$$M_{bx} = M_{bWx} + M_{bHx} \cdot k_1 \cdot k_3 + M_{bEx} \cdot k_2 \tag{9}$$

Under natural condition, k_1 and k_2 are both equal to 0. Under rainfall conditions, $k_1 = 0$. Under earthquake conditions, $k_2 = 0$. For the case of two free faces, $k_3 = 1$; for the case of three free surfaces, $k_3 = 0$. Based on bending theory (Adrian, 2010), eccentricity distance along x direction (e_x) can be expressed as,

$$e_x = \frac{M_{bx}}{N_z} = \frac{M_{bWx} + M_{bHx} \cdot k_1 \cdot k_3 + M_{bEx} \cdot k_2}{W \cos\alpha - (H_x \cdot k_1 \cdot k_3 + E_x \cdot k_2) \sin\theta_1 - \left(H_y \cdot k_1 + E_y \cdot k_2\right) \sin\theta_1} \tag{10}$$

The same method can be used to obtain e_y,

$$e_y = \frac{M_{by}}{N_z} = \frac{M_{bWy} + M_{bHy} \cdot k_1 + M_{bEy} \cdot k_2}{W \cos\alpha - (H_x \cdot k_1 \cdot k_3 + E_x \cdot k_2) \sin\theta_1 - \left(H_y \cdot k_1 + E_y \cdot k_2\right) \sin\theta_1} \tag{11}$$

According to the stress distribution of rectangular shape foundation (Adrian, 2010), the stress in the (x, y) coordinates, $p(x, y)$, results to be,

$$p(x,y) = \frac{N}{A} + \frac{Ne_x}{I_y}x + \frac{Ne_y}{I_x}y \tag{12}$$

With the formulas,

$$I_x = \frac{(a - d_1)(b - d_2)^3}{12} \tag{13}$$

$$I_y = \frac{(b - d_2)(a - d_1)^3}{12} \tag{14}$$

$$A = (a - d_1 - d_3)(b - d_2) \tag{15}$$

by substituting Eq. (13-15) into Eq. (12), $p(x, y)$ can be derived as,

$$p(x,y) = \frac{N}{A}\left[1 + \frac{12e_x}{(a - d_1 - d_3)^2}x + \frac{12e_y}{(b - d_2)^2}y\right] \quad x \in \left[-\frac{a - d_1 - d_3}{2}, \frac{a - d_1 - d_3}{2}\right], y \in \left[-\frac{b - d_2}{2}, \frac{b - d_2}{2}\right] \tag{16}$$

p_{max} and p_{mim} can be derived from Eq. (16) as,

$$p_{max} = p\left(\frac{a - d_1 - d_3}{2}, \frac{b - d_2}{2}\right) \tag{17}$$

https://doi.org/10.5194/egusphere-2022-658
Preprint. Discussion started: 25 July 2022

$$p_{min} = p\left(-\frac{a-d_1-d_3}{2}, -\frac{b-d_2}{2}\right) \tag{18}$$

The mudstone foundation has both the compressive strength and tensile strength, so the value of $p(x,y)$ is modified to obtain two piecewise functions,

$$p_p(x,y) = \begin{cases} \sigma_{cmax}, & p(x,y) \geq \sigma_{cmax} \\ p(x,y), & 0 < p(x,y) \leq \sigma_{cmax} \\ 0, & p(x,y) < 0 \end{cases} \tag{19}$$

$$p_n(x,y) = \begin{cases} 0, & p(x,y) < -\sigma_{tmax} \\ p(x,y), & -\sigma_{tmax} \leq p(x,y) < 0 \\ 0, & p(x,y) \geq 0 \end{cases} \tag{20}$$

$p_p(x,y)$ provides support normal force for the underlying sandstone, and $p_n(x,y)$ provides tension force.

3.2.2 Calculation of factors of safety

According to the principle of friction, the ultimate Shear Strength τ_{max} results to be,

$$\tau_{max} = \int_{-\frac{a-d_1-d_3}{2}}^{\frac{a-d_1-d_3}{2}} \int_{-\frac{b-d_2}{2}}^{\frac{b-d_2}{2}} \left[p_p(x,y)\tan\varphi + c\right] dy\, dx \tag{21}$$

Therefore, the Fos against sliding, Fos_{sl}, can be defined as,

$$Fos_{sl} = \frac{S_{stabilizing}}{S_{sliding}} = \frac{\tau_{max}}{W|\sin\alpha_s| + H_x \cdot \cos\omega_s \cdot \cos\alpha_s \cdot k_1 \cdot k_3 + H_y \cdot |\sin\omega_s| \cdot \cos\alpha_s \cdot k_1 + E \cdot \cos\alpha_s \cdot k_2} \tag{22}$$

When the block can slide freely, $\alpha_s = \alpha$, $\omega_s = 0$; when the block is constrained to slide along a joint plane (e.g., J1), $\alpha_s = \theta_1\ or\ \theta_2$, $\omega_s = \omega_1\ or\ \omega_2$. For the case of anaclinal slope, Fos_{sl} is not exist.

With regard to stability against toppling, along x direction, the part of the block above the mudstone base provides the stabilizing moment $M_{W_{inx}}$, and the part of the block above the cavity provides the overturning moment $M_{W_{outx}}$. When the tension exists, there will be an additional stabilizing moment. M_{px}, $M_{W_{inx}}$, $M_{W_{outx}}$ and M_{px}can be derived as,

$$M_{W_{inx}} = W\frac{a-d_1}{a}\cos\theta_1 \cdot \left(\frac{a-d_1}{2}\right) \tag{23}$$

$$M_{W_{outx}} = W\frac{d_1}{a}\cos\theta_1 \cdot \frac{d_1}{2} \tag{24}$$

$$M_{px} = -\int_{-\frac{b-d_2}{2}}^{\frac{b-d_2}{2}} \int_{-\frac{a-d_1-d_3}{2}}^{\frac{a-d_1-d_3}{2}} p_n(x,y) \cdot \left(\frac{a}{2} - d_1 - x\right) dx\, dy \tag{25}$$

And M_{Hx}, M_{Ex} can be derived as,

$$M_{Hx} = \int_{-\frac{b-d_2}{2}}^{\frac{b-d_2}{2}} \int_0^{h_w\cos\theta_1} \gamma_w \left(h_w - \frac{z}{\cos\theta_1}\right)\left(\frac{z}{\cos\theta_1} + (a-d_1)\sin\theta_1\right) dz dy \tag{26}$$

$$M_{Ex} = E_x\left(\frac{h}{2} + \left(\frac{a}{2} - d_1\right)\sin\theta_1\right) \tag{27}$$

https://doi.org/10.5194/egusphere-2022-658
Preprint. Discussion started: 25 July 2022

Therefore, the Fos against toppling along x direction, Fos_{tox}, results to be,

$$Fos_{tox} = \frac{M_{stabilizing}}{M_{overturning}} = \frac{M_{W_{inx}} + M_{px}}{M_{W_{outx}} + M_{Hx} \cdot k_1 \cdot k_3 + M_{Ex} \cdot k_2} \quad (28)$$

Similarly, the Fos_{toy} can be obtained,

$$Fos_{toy} = \frac{M_{stabilizing}}{M_{overturning}} = \frac{M_{W_{iny}} + M_{py}}{M_{W_{outy}} + M_{Hy} \cdot k_1 + M_{Ey} \cdot k_2} \quad (29)$$

The smaller value is selected as the Fos of toppling failure mode, Fos_{to},

$$Fos_{to} = min(Fos_{tox}, Fos_{toy}) \quad (30)$$

When the stress on mudstone exceeds its strengths, it has partial damage and decrease the stability of rock block. Therefore, the Fos with the consideration of compressive strength (Fos_{co}) and tensional strength (Fos_{te}) can be derived as,

$$Fos_{co} = \frac{\sigma_{tmax}}{p_{max}} \quad (31)$$

$$Fos_{te} = \frac{\sigma_{cmax}}{-p_{min}} \quad (32)$$

Finally, four Fos of unstable rock block were obtained. Fos_{sl} and Fos_{to} are routine indicators about sandstone blocks that directly characterize its stability. Fos_{co} and Fos_{te} are two indicators proposed in this study, which describe the state of underlying mudstone base. It is necessary to aggregate four Fos to judge the stability of unstable rock mass. The entire calculation process is shown in Fig. 9.

https://doi.org/10.5194/egusphere-2022-658
Preprint. Discussion started: 25 July 2022

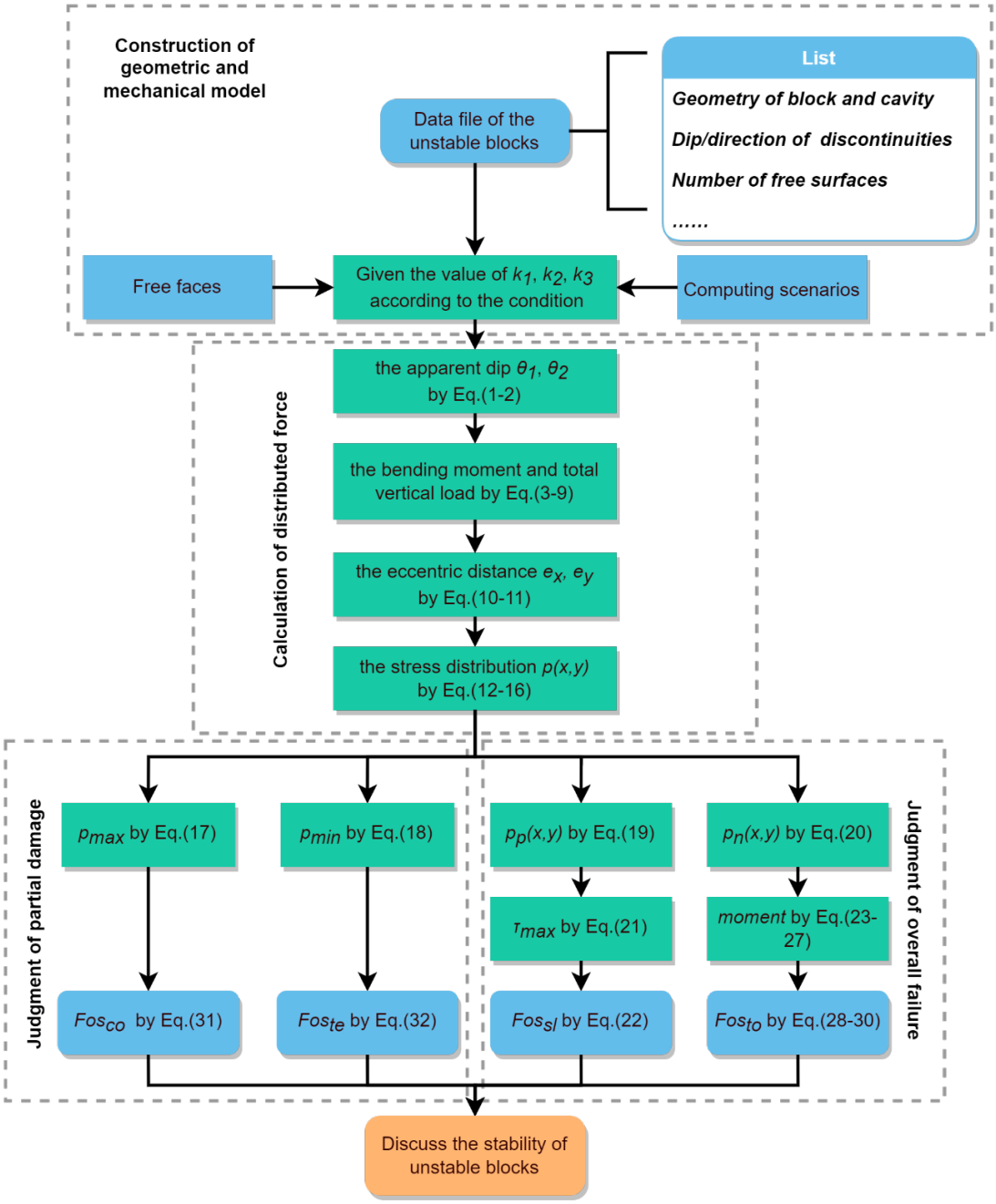

Figure 9 The calculation process of Fos of the unstable rock blocks.

4 Parameters and results

https://doi.org/10.5194/egusphere-2022-658
Preprint. Discussion started: 25 July 2022

A detailed field investigation was carried out in the source area of rockfall (Fig. 3d and 4a). The size of the blocks is determined by on-site measurement with tape and laser rangefinder. The basal cavities in mudstone were measured with a steel ruler, and the morphological characteristics of mudstone foundation are mainly described with the average erosion depth of the cavity. The attitude of discontinuities was measured by compass. The mechanical parameters for Fos calculation of blocks are abundantly recorded in the investigation reports and published literatures in this area. The unit weight of sandstone block (γ_s) is 25 kN/m^3 (Tang et al., 2010), the friction angle of the contact surface (φ) is set to be 25° and the cohesion (c) is set to be 70 kPa (Zhang et al., 2016). Because of the strength degradation of mudstone foundation due to intense weathered, maximum compressive stress of mudstone (σ_{cmax}) is replaced by the bearing capacity of mudstone foundation (2300 kPa), which is obtained through plate load test in adjacent area (Zheng et al., 2021). Besides, maximum tensile stress of mudstone (σ_{tmax}) is one ninth of σ_{cmax}. The height of water level (h_w) is set to be one-third of h, and an earthquake contribution coefficient k_e of 0.05 is considered in stability calculations. The calculated geometric parameters and Fos results are shown in Table 2.

276 **Table 2** Geometric parameters and Fos results obtained from the analytical method in section 3.

Block	Free	h	a	b	d_1	d_2	d_3	α	Dip direction [°]			NS					RS				ES			
number	faces	[m]	[m]	[m]	[m]	[m]	[m]	[°]	BD	J1	J2	Fos_{te}	Fos_{co}	Fos_{sl}	Fos_{to}	Fos_{min}	Fos_{te}	Fos_{co}	Fos_{sl}	Fos_{to}	Fos_{te}	Fos_{co}	Fos_{sl}	Fos_{to}
W01	3	23	7.2	6.1	0.65	0.25	0.17	6	78	7	97	-	2.99	5.61	101.54	2.99	-	2.56	3.18	11.91	0.90	1.63	3.81	4.88
W02	3	23	6.42	5.25	0.78	0.4	0.31	16	148	51	141	-	2.84	2.10	52.28	2.10	-	2.33	1.54	8.49	0.51	1.48	1.82	3.79
W03	2	20	3.5	2.6	0.84	0.55	-	7	341	53	143	0.52	1.56	16.53	4.72	0.52	0.15	0.86	2.83	1.02	0.14	0.81	9.12	1.01
W04	2	19	4.6	4.6	0.62	0.77	-	7	273	65	155	7.35	2.37	-	24.74	2.37	0.80	1.81	-	6.83	0.35	1.38	-	3.23
W05	2	15	16.7	5.6	2.13	1.36	-	5	283	50	140	1.70	2.57	-	9.86	1.70	1.19	2.39	-	6.10	0.63	1.99	-	3.36
W06	3	20	16.7	9.7	7.5	4.2	3.9	5	302	226	316	0.15	0.87	8.67	1.53	0.15	0.15	0.84	4.73	1.52	0.12	0.72	5.96	1.16
W07	2	22	9.2	3.7	0.64	0.8	-	12	324	315	405	-	2.27	2.82	22.86	2.27	0.57	1.55	1.62	2.97	0.34	1.28	2.44	2.21
W08	2	23	12	7.9	2	1.9	-	3	317	332	422	0.76	1.55	11.75	8.99	0.76	0.51	1.40	4.51	5.09	0.29	1.14	6.29	2.84
W09	2	18	8.4	6	0.9	2.5	-	8	60	335	425	0.38	1.48	4.98	2.23	0.38	0.29	1.30	2.87	1.56	0.22	1.12	4.08	1.20
W10	2	23	5.7	3.3	1.3	0.85	-	5	329	313	403	0.30	1.16	7.41	2.53	0.30	0.12	0.71	2.30	0.71	0.11	0.68	5.84	0.75
W11	3	22	1.1	2	0.1	0.64	0.1	4	327	120	210	1.13	1.74	19.08	4.97	1.13	0.12	0.69	2.37	0.51	0.07	0.49	10.57	0.73
W12	2	25	3.9	4	0.74	0.96	-	12	355	297	387	0.64	1.44	2.78	10.36	0.64	0.15	0.82	1.48	1.81	0.14	0.75	2.70	1.61
W13	2	12	11.9	10.9	3	2.28	-	7	36	73	163	1.06	2.77	7.28	9.39	1.06	0.99	2.71	5.63	9.02	0.70	2.41	4.93	5.65
W14	3	19	13	5	0	1.1	0	8	296	73	163	-	2.67	6.40	12.57	2.67	3.75	2.28	3.09	5.15	0.68	1.75	4.41	2.94
W15	2	18	22	6	8.3	0	-	8	351	200	290	0.70	1.84	9.74	2.93	0.70	0.60	1.75	5.03	2.83	0.39	1.50	5.79	2.34
W16	3	11	5.2	7.6	0	2.9	0	13	42	144	234	1.09	3.04	3.46	3.65	1.09	1.01	2.96	2.84	3.45	0.62	2.45	2.98	2.45
W17	3	7	8	2	0	0.56	0	20	30	156	246	7.71	6.72	3.07	6.83	3.07	3.40	5.87	2.29	4.49	1.48	4.70	2.81	2.86
W18	2	12	8.5	4.5	1.61	1.27	-	2	252	253	343	0.97	2.66	20.49	7.05	0.97	0.75	2.46	10.06	4.50	0.50	2.08	8.90	2.82
W19	2	15	4.2	5.2	1.6	0.68	-	5	28	56	146	0.75	2.12	8.71	5.49	0.75	0.48	1.80	4.17	3.66	0.31	1.48	5.79	2.24
W20	3	15	1.8	1.7	0.23	0.5	0.3	4	20	63	153	7.96	2.95	9.44	6.08	2.95	0.29	1.43	3.39	0.87	0.18	1.07	7.12	1.03
W21	3	20	18.9	9	0	2	0	7	348	71	161	-	2.51	4.96	12.25	2.51	-	2.36	3.31	7.48	1.15	1.90	3.58	3.95
W22	2	7	5.4	5.7	1	1.65	-	6	294	53	143	1.53	4.48	-	5.78	1.53	1.44	4.38	-	5.37	1.00	3.81	-	3.88

277 Note: (-) means the value is not existing. NS-Natural scenarios, RS- Rainfall scenarios, ES-Earthquake scenarios.

278

https://doi.org/10.5194/egusphere-2022-658
Preprint. Discussion started: 25 July 2022

5 Discussion

5.1 Distribution Characteristics of Fos

There are up to 12 results of Fos per unstable block with the consideration of three scenarios and four failure modes (i.e., partial damage and overall failure). Most of Fos_{te} are less than 1 in any scenarios (purple points in Fig.10), except for two blocks (i.e., W17 and W20), whose Fos_{te} are also close to 1 under rainfall or earthquake scenarios. Although most of Fos_{co} (green points in Fig.10) are greater than 1, they are closer to the critical state of $Fos = 1$ than Fos_{sl} and Fos_{to} (represented by blue and yellow points in Fig.10, respectively). According to the results, their Fos_{te} and Fos_{co} are less than 1 or close to 1, which means that the underlying mudstone has been partially damaged due to slight compressive or tensile failure, and the blocks are potential unstable with the current depth of basal cavity. However, most of the blocks do not exhibit the overall failure, and they still exist on the slope. Meanwhile, their Fos_{sl} and Fos_{to} are greater than 1 in different scenarios, which is consistent with the actuality. Due to the uncertainty of mechanical parameters, it is possible that most of the blocks are in a critical state, in which they are partially damaged but the whole block is still stable.

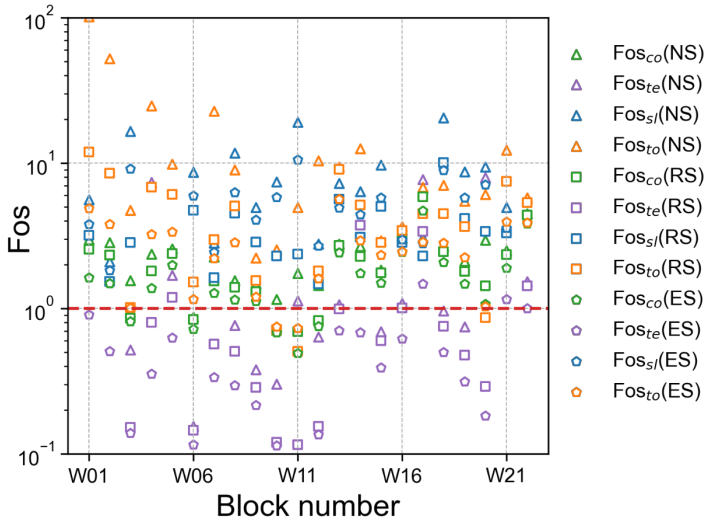

Figure 10 Distribution of Fos in different scenarios. Shapes represent different scenarios and colors represent different failure modes.

5.2 Relationship between Fos and geometric parameters

Fig. 11 presents the relationship between Fos_{min} and two main geometric parameters. In general, the dip angle of the bedding plane (α) is the key factor influencing the sliding failure mode. The horizontal axis in Fig. 11a is α between rock blocks and underlying mudstone. Most of the points in Fig. 11a are in the interval [0, 8], which is consistent with the feature of sub-horizontal stratum in the study area. The shade of the points does not change significantly in the x-axis direction, which indicates that the dip of contact surface has little correlation with rockfall stability in this area. There was a significant

https://doi.org/10.5194/egusphere-2022-658
Preprint. Discussion started: 25 July 2022

positive correlation between the retreat ratio (r_{max}) and Fos_{min} as Fig. 11b shown. In Fig. 11b, all the points can be clearly divided into two parts by a red dashed line, Fos_{min} of the points in the upper part are all lower than the critical state ($Fos = 1$). Therefore, if r_x and r_y can be obtained through the detailed field investigation, the block stability can be preliminarily determined by the formula in the Fig. 11b.

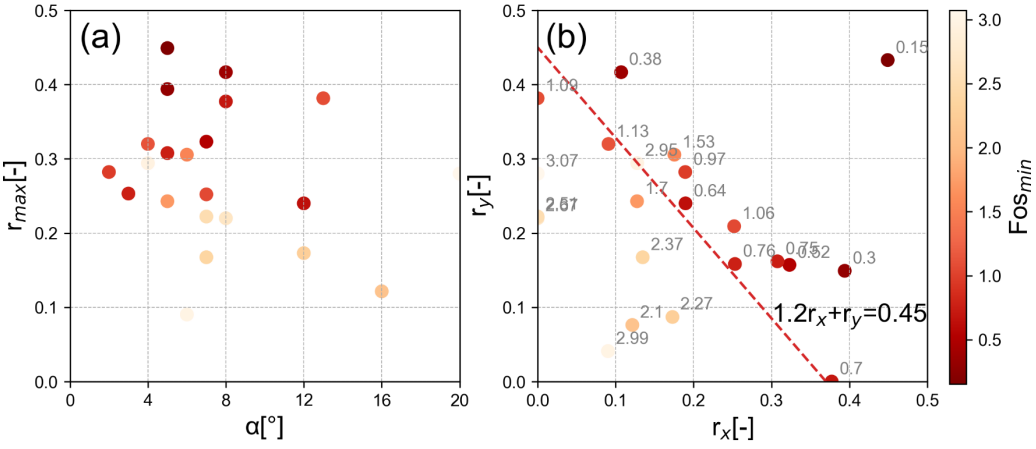

Figure 11 The relationship between Fos and main geometric parameters. α is the dip angle of the contact surface between rock block and underlaying mudstone. r_x and r_y are the retreat ratio along x direction and y direction, respectively, equal to d_1/a and d_2/b. r_{max} is the larger one of r_x and r_y.

5.3 Definition of rockfall susceptibility

In order to explore the variation of Fos with the progressive erosion process of cavity on the blocks, the cavity retreat velocities in different directions are assumed to be equal (5mm/year, Zhang et al. (2016)). The rockfall evolution also can be well displayed from Fig. 12. The instability of the blocks starts from the failure (or damage) of the foundation. Fos_{te} and Fos_{co} reach critical state much earlier than Fos_{sl} and Fos_{to}. This result is consistent with Fig. 10, in which 90.9% of the purple and green points (Fos_{te} and Fos_{co}) are near the line of $Fos = 1$. This result also well agrees with the field insight, that is most rock blocks are potential unstable and many fractures appear in the mudstone. Even if Fos_{sl} or Fos_{to} is higher than 1, in fact its foundation has begun to be damaged. In the case of heavy rain or earthquake, Fos_{sl} and Fos_{to} may be less than 1, and the rockfall will occur.

https://doi.org/10.5194/egusphere-2022-658
Preprint. Discussion started: 25 July 2022

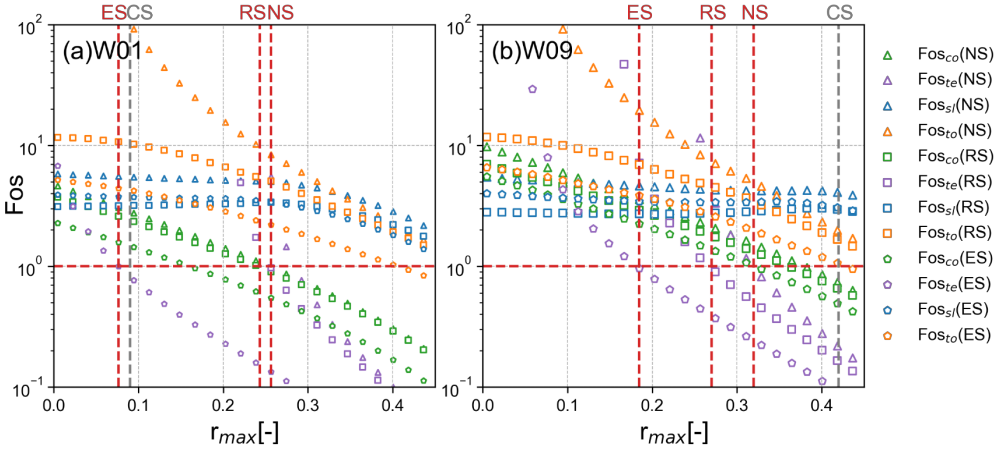

Figure 12 Variation of Fos with r_{max}. (a) and (b) are the results for W01 and W09, respectively, which represent the situation of the blocks with two and three free faces. The gray dotted line (CS) approximately represents the current state of the unstable blocks. The red dotted lines correspond to the critical values of r in different scenarios.

Based on the above analysis, rockfall susceptibility can be divided into three levels. When both Fos_{co} and Fos_{te} are greater than 1, the overall rock block is stable and the mudstone base is not damaged, which is defined as "low susceptibility" and represented by the green area in the Fig. 13. With the development of the cavity erosion, when Fos_{co} or Fos_{te} is less than 1 and Fos_{sl} and Fos_{to} are higher than 1, the base begins to be damaged and the overlying sandstone blocks still maintain relatively stable. This state is defined as "moderate susceptibility" and represented by the orange area. When Fos_{sl} or Fos_{to} is less than 1 in some scenarios, the rock blocks are in a "high susceptibility" state which means that rockfalls are highly likely to occur. Fig. 13a indicates that along with the increase of cavity retreat ratio, the susceptibility of W01 and W09 changes from low susceptibility to moderate susceptibility in natural scenario. As Fig. 13b and c shown, when rainfall or earthquake occurs, Fos_{sl} or Fos_{to} of some blocks are less than 1, which means that some blocks have evolve to the state of high susceptibility and the overall sandstone blocks are unstable.

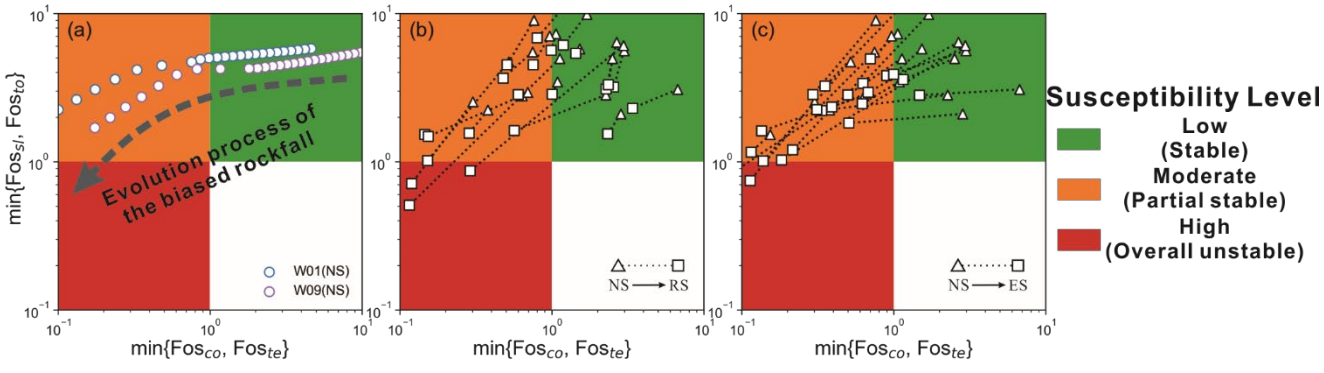

Figure 13 Rockfall susceptibility based on Fos distribution. The susceptibility is defined as three levels, represented by red, orange and green respectively. (a) shows the progressive failure process of rock block changing from low susceptibility to moderate susceptibility, as

https://doi.org/10.5194/egusphere-2022-658
Preprint. Discussion started: 25 July 2022

the increase of cavity retreat ratio (illustrated by W01 and W09 in natural scenario. (b) and (c) show the change of susceptibility of biased rock blocks, when the scenario changes from natural condition to rainfall and earthquake conditions.

5.4 Critical retreat ratio in the study area

The cavity plays an important role in the progressive failure process of biased rockfall. In order to analyze the effect of retreat ratio on the stability of rock blocks, all blocks in the study area were selected to calculated their Fos and susceptibility level with the increased r, whose retreat velocity in different directions are assumed to be equal. Fig. 14 shows that along with the increase of retreat ratio, the susceptibility level of rock blocks changes from low to moderate susceptibility. Corresponding to the critical state of $\min\{Fos_{co}, Fos_{te}\} = 1$ of all blocks, the minimum retreat ratio is 0.2565, and the maximum retreat ratio is 0.4050, which are marked by vertical gray dotted line in the Fig. 14. According to the statistics analysis of critical retreat ratios, the mean and median are 0.3318 and 0.3308, respectively. Therefore, the critical retreat rate of the rock blocks in the study area is determined to be 0.33, which is marked by vertical red dotted line in the Fig. 14. This result could provide evidence for field investigation and regional risk control of biased rockfall. The rock blocks with a retreat ratio exceeding 0.33 can be regarded as probable rockfall source, which should be prevented with the highest priority. For unstable rock blocks in sub-horizontal formation, filling the cavity with a support structure is an effective mitigation measure.

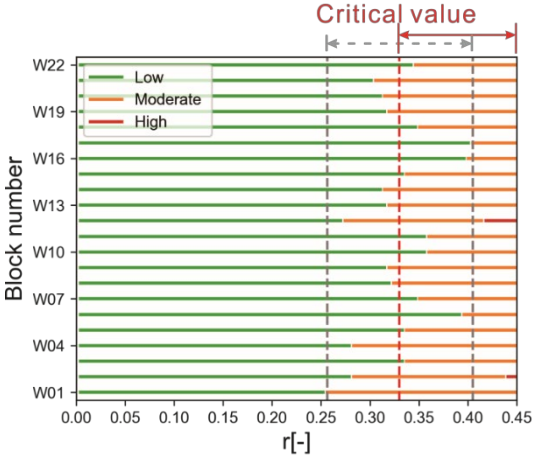

Figure 14 The effect of retreat ratio on the Fos of rock block, which is illustrated by all blocks in the study area. The critical value of r is 0.33.

6 Conclusion

Rockfall usually causes amounts of monetary damage and death in mountainous area. For the biased rockfall in sub-horizontal formations, the traditional LEM method usually overestimates the stability of rock blocks with natural cavities. The aim of this study was to present a new three-dimensional analytical method for the stability of rock block with basal

https://doi.org/10.5194/egusphere-2022-658
Preprint. Discussion started: 25 July 2022

cavity. In the geological model, a non-uniform distributed force due to eccentric effect is applied at the contact surface, in place of a point force. The method considers four failure modes according to the rockfall evolution process, including partial damage of soft foundation and overall failure of rock block. The proposed method was used to calculate Fos of the typical unstable rock blocks in the study area. The results are consistent with the natural states of the rock blocks. Besides, the statistical analysis indicates that retreat ratio is the crucial factor influencing the Fos of biased rockfall. The critical retreat ratio from low to moderate rockfall susceptibility is 0.33.

The proposed method improves the three-dimensional geomechanical model of rock block with basal cavity, by considering non-uniform distributed force at the contact surface, which could promote the accuracy of rockfall stability analysis. However, because of the complexity of mechanical failure mechanism of biased rockfall and the assumptions adopted in the method, it is essential to highlight the limitations of this method. In the proposed method, the contact surface between rock block and underlying mudstone is assumed to be a rectangle. However, in reality its natural shape is irregular, which results in complex distribution of supporting force. In addition, in the geomechanical model, the failure surface of biased rockfall is set to be the contact surface of rock block and mudstone. However, the natural failure surface may be formed along the cleavages in the mudstone, which will lead to the changes in mechanical parameters of stability analysis. Further research is clearly needed for the improvement of geomechanical model of biased rockfall

Data availability

All raw data can be provided by the corresponding authors upon request.

Author contributions

XS, BC and JD planned the campaign; XS and BC performed the field measurements; XS, BC, WW and BL designed and developed the methodology. XS, BC and JD analyzed the data; XS and BC wrote the manuscript draft; JD and WW reviewed and edited the manuscript.

Competing interests

The authors declare that they have no conflict of interest.

Acknowledgements

This research is funded by the National Natural Science Foundation of China (No. 42172318 and No. 42177159). The fist author thanks Master Chengjie Luo and Yu Wang for data collection in the field. We also thank the assistance of the Research Center of Geohazard Monitoring and Warning in the Three Gorges Reservoir, China.

https://doi.org/10.5194/egusphere-2022-658
Preprint. Discussion started: 25 July 2022

References

Adrian, I.: Pressures distribution for eccentrically loaded rectangular footings on elastic soils, Proceedings of the 2010 international conference on Mathematical models for engineering science, Tenerife, Spain, 213–216,

Alejano, L. R., Carranza-Torres, C., Giani, G. P., and Arzua, J.: Study of the stability against toppling of rock blocks with rounded edges based on analytical and experimental approaches, Eng. Geol., 195, 172-184, https://doi.org/10.1016/j.enggeo.2015.05.030, 2015.

Alejano, L. R., Ordóñez, C., Armesto, J., and Rivas, T.: Assessment of the instability hazard of a granite boulder, Nat. Hazards, 53, 77-95, https://doi.org/10.1007/s11069-009-9413-0, 2010.

Ashby, J.: Sliding and toppling modes of failure in models and jointed rock slopes, M.S. thesis, Imperial College London University, London, 1971.

Bray, J. W. and Goodman, R. E.: The theory of base friction models, Int J Rock Mech Min Sci Geomech Abstr, 18, 453-468, https://doi.org/10.1016/0148-9062(81)90510-6, 1981.

Budetta, P.: Assessment of rockfall risk along roads, Nat. Hazards Earth Syst. Sci., 4, 71-81, https://doi.org/10.5194/nhess-4-71-2004, 2004.

Budetta, P. and Nappi, M.: Comparison between qualitative rockfall risk rating systems for a road affected by high traffic intensity, Nat. Hazards Earth Syst. Sci., 13, 1643-1653, https://doi.org/10.5194/nhess-13-1643-2013, 2013.

Chau, K. T., Wong, R. H. C., Liu, J., and Lee, C. F.: Rockfall hazard analysis for Hong Kong based on rockfall inventory, Rock Mech. Rock Eng., 36, 383-408, https://doi.org/10.1007/s00603-002-0035-z, 2003.

Chen, H. K. and Tang, H. M.: Stability analysis method of perilous rock in source of avalanche, J. Geol. Min. Res., 2, 60-67, https://doi.org/10.5897/JGMR.9000070, 2010.

Chen, H. K., Xian, X. F., Tang, H. M., and Feng, Q. H.: A massive development mechanism and countermeasures for perilous rocks in the Three Gorges Reservoir area of PR China: The example of the Taibaiyan cliff at Wanzhou, Journal of Chongqing University, 31, 1178-1184, 2008.

Corominas, J., Mavrouli, O., and Ruiz-Carulla, R.: Magnitude and frequency relations: are there geological constraints to the rockfall size?, Landslides, 15, 829-845, https://doi.org/10.1007/s10346-017-0910-z, 2018.

Cruden, D. M. and Varnes, J. D.: Landslide types and processes. Landslides: investigation and mitigation, transportation research board (National Research Council), National Academy Press, Washington, DC, 1996.

D'Amato, J., Hantz, D., Guerin, A., Jaboyedoff, M., Baillet, L., and Mariscal, A.: Influence of meteorological factors on rockfall occurrence in a middle mountain limestone cliff, Nat. Hazards Earth Syst. Sci., 16, 719-735, https://doi.org/10.5194/nhess-16-719-2016, 2016.

Derron, M. H., Jaboyedoff, M., and Blikra, L. H.: Preliminary assessment of rockslide and rockfall hazards using a DEM (Oppstadhornet, Norway), Nat. Hazards Earth Syst. Sci., 5, 285-292, https://doi.org/10.5194/nhess-5-285-2005, 2005.

https://doi.org/10.5194/egusphere-2022-658
Preprint. Discussion started: 25 July 2022

Ferrari, F., Giacomini, A., and Thoeni, K.: Qualitative Rockfall Hazard Assessment: A Comprehensive Review of Current Practices, Rock Mech. Rock Eng., 49, 2865-2922, https://doi.org/10.1007/s00603-016-0918-z, 2016.

Frattini, P., Crosta, G., Carrara, A., and Agliardi, F.: Assessment of rockfall susceptibility by integrating statistical and physically-based approaches, Geomorphology, 94, 419-437, https://doi.org/10.1016/j.geomorph.2006.10.037, 2008.

Frayssines, M. and Hantz, D.: Modelling and back-analysing failures in steep limestone cliffs, Int. J. Rock Mech. Min. Sci., 46, 1115-1123, https://doi.org/10.1016/j.ijrmms.2009.06.003, 2009.

Guzzetti, F., Reichenbach, P., and Wieczorek, G. F.: Rockfall hazard and risk assessment in the Yosemite Valley, California, USA, Nat. Hazards Earth Syst. Sci., 3, 491-503, https://doi.org/10.5194/nhess-3-491-2003, 2003.

Hutchinson, J. N.: Field and laboratory studies of a fall in Upper Chalk cliffs at Joss Bay, Isle of Thanet, in: Stress-Strain Behaviour of Soils, Proceedings of the Roscoe Memorial Symposium, Oxfordshire, 29-31 March 1971, 692-706, 1972.

Jaboyedoff, M., Baillifard, F., Philippossian, F., and Rouiller, J. D.: Assessing fracture occurrence using "weighted fracturing density": a step towards estimating rock instability hazard, Nat. Hazards Earth Syst. Sci., 4, 83-93, https://doi.org/10.5194/nhess-4-83-2004, 2004.

Jaboyedoff, M., Ben Hammouda, M., Derron, M.-H., Guérin, A., Hantz, D., and Noel, F.: The Rockfall Failure Hazard Assessment: Summary and New Advances, in: Understanding and Reducing Landslide Disaster Risk: Volume 1 Sendai Landslide Partnerships and Kyoto Landslide Commitment, edited by: Sassa, K., Mikoš, M., Sassa, S., Bobrowsky, P. T., Takara, K., and Dang, K., Springer International Publishing, Cham, 55-83, https://doi.org/10.1007/978-3-030-60196-6_3, 2021.

Kogure, T., Aoki, H., Maekado, A., Hirose, T., and Matsukura, Y.: Effect of the development of notches and tension cracks on instability of limestone coastal cliffs in the Ryukyus, Japan, Geomorphology, 80, 236-244, https://doi.org/10.1016/j.geomorph.2006.02.012, 2006.

Kromer, R., Lato, M., Hutchinson, D. J., Gauthier, D., and Edwards, T.: Managing rockfall risk through baseline monitoring of precursors using a terrestrial laser scanner, Can. Geotech. J., 54, 953-967, https://doi.org/10.1139/cgj-2016-0178, 2017.

Malamud, B. D., Turcotte, D. L., Guzzetti, F., and Reichenbach, P.: Landslide inventories and their statistical properties, Earth Surf. Proc. Land., 29, 687-711, https://doi.org/10.1002/esp.1064, 2004.

Matasci, B., Stock, G. M., Jaboyedoff, M., Carrea, D., Collins, B. D., Guerin, A., Matasci, G., and Ravanel, L.: Assessing rockfall susceptibility in steep and overhanging slopes using three-dimensional analysis of failure mechanisms, Landslides, 15, 859-878, https://doi.org/10.1007/s10346-017-0911-y, 2018.

Pérez-Rey, I., Muñiz-Menéndez, M., González, J., Vagnon, F., Walton, G., and Alejano, L. R.: Laboratory physical modelling of block toppling instability by means of tilt tests, Eng. Geol., 282, 105994, https://doi.org/10.1016/j.enggeo.2021.105994, 2021.

Pierson, L. A., Davis, S. A., and Van Vickle, R.: Rockfall hazard rating system–implementation manual, Federal Highway Administration (FHWA), Report FHWA—OR-EG-90-01, FHWA, US Department of Transportation, 80 pp., 1990.

https://doi.org/10.5194/egusphere-2022-658
Preprint. Discussion started: 25 July 2022

Sagaseta, C.: On the Modes of Instability of a Rigid Block on an Inclined Plane, Rock Mech. Rock Eng., 19, 261-266, https://doi.org/10.1007/Bf01039998, 1986.

Santi, P. M., Russell, C. P., Higgins, J. D., and Spriet, J. I.: Modification and statistical analysis of the Colorado Rockfall Hazard Rating System, Eng. Geol., 104, 55-65, https://doi.org/10.1016/j.enggeo.2008.08.009, 2009.

Tang, H. M., Wang, L. F., Chen, H. K., and Xian, X. F.: Collapse sequence of perilous rock on cliffs with soft foundation, Chinese Journal of Geotechnical Engineering, 32, 205-210, 2010.

Volkwein, A., Schellenberg, K., Labiouse, V., Agliardi, F., Berger, F., Bourrier, F., Dorren, L. K. A., Gerber, W., and Jaboyedoff, M.: Rockfall characterisation and structural protection - a review, Nat. Hazards Earth Syst. Sci., 11, 2617-2651, https://doi.org/10.5194/nhess-11-2617-2011, 2011.

Ward, D. J., Berlin, M. M., and Anderson, R. S.: Sediment dynamics below retreating cliffs, Earth Surf. Proc. Land., 36, 1023-1043, https://doi.org/10.1002/esp.2129, 2011.

Wu, L. Z., Zhang, L. M., Zhou, Y., Xu, Q., Yu, B., Liu, G. G., and Bai, L. Y.: Theoretical analysis and model test for rainfall-induced shallow landslides in the red-bed area of Sichuan, Bull. Eng. Geol. Environ., 77, 1343-1353, https://doi.org/10.1007/s10064-017-1126-0, 2018.

Yu, B., Ma, E., Cai, J., Xu, Q., Li, W., and Zheng, G.: A prediction model for rock planar slides with large displacement triggered by heavy rainfall in the Red bed area, Southwest, China, Landslides, 18, 773-783, https://doi.org/10.1007/s10346-020-01528-x, 2021.

Zhan, J., Yu, Z., Lv, Y., Peng, J., Song, S., and Yao, Z.: Rockfall Hazard Assessment in the Taihang Grand Canyon Scenic Area Integrating Regional-Scale Identification of Potential Rockfall Sources, Remote sens. (Basel). 14, 3021, https://doi.org/10.3390/rs14133021, 2022.

Zhang, K., Tan, P., Ma, G. W., and Cao, P.: Modeling of the progressive failure of an overhang slope subject to differential weathering in Three Gorges Reservoir, China, Landslides, 13, 1303-1313, https://doi.org/10.1007/s10346-015-0672-4, 2016.

Zhang, M., Yin, Y. P., and Huang, B. L.: Mechanisms of rainfall-induced landslides in gently inclined red beds in the eastern Sichuan Basin, SW China, Landslides, 12, 973-983, https://doi.org/10.1007/s10346-015-0611-4, 2015.

Zheng, L. N., Chen, J. B., Zhou, Q. J., Feng, S. Q., Luo, Y. B., and Shen, P.: Experimental study on bearing capacity of moderately weathered mudstone in Chengdu area, Chinese Journal of Geotechnical Engineering, 43, 926-932, https://doi.org/10.11779/CJGE202105017, 2021.

Zhou, C., Yin, K. L., Cao, Y., Ahmed, B., Li, Y. Y., Catani, F., and Pourghasemi, H. R.: Landslide susceptibility modeling applying machine learning methods: A case study from Longju in the Three Gorges Reservoir area, China, Comput Geotech, 112, 23-37, https://doi.org/10.1016/j.cageo.2017.11.019, 2018.

Zhou, Y., Shi, S., Zhang, Y., Cai, Q., Liang, J., and Cheng, Y.: Stability of unstable rock in nearly-horizontal sandstone-mudstone stratum due to enlarged rock-cell, Journal of Engineering Geology, 25, 1220-1229, https://doi.org/10.13544/j.cnki.jeg.2017.05.006, 2017.